# Modeling the optical constants of $Hg_xCd_{1-x}Te$ alloys in the 1.5–6.0 eV range

Aleksandra B. Djurišić and E. Herbert Li[a)]
*Department of Electrical and Electronic Engineering, University of Hong Kong, Pokfulam Road, Hong Kong*

(Received 17 September 1998; accepted for publication 3 December 1998)

The optical constants of $Hg_xCd_{1-x}Te$ as a function of energy and composition $x$ are modeled over a wide spectral range from 1.5 to 6 eV. The model employed represents an extension of Adachi's model and incorporates the adjustable broadening function rather than the conventional Lorentzian one. In this way, greater flexibility of the model is achieved, enabling us to obtain an excellent agreement with the experimental data. The relative rms errors obtained for all compositions are below 2.5% for the real part and below 6% for the imaginary part of the index of refraction. The lowest rms errors are obtained for $x=0$ (0.6% for the real part and 0.7% for the imaginary part of the index of refraction), and the highest for the $x=0.91$ (2.4% for the real part and 5.8% for the imaginary part). © *1999 American Institute of Physics.* [S0021-8979(99)05105-1]

## I. INTRODUCTION

$Hg_xCd_{1-x}Te$ represents a substitutional pseudobinary alloy. It has high electron mobility and its fundamental absorption edge can vary with composition $x$ over a substantial part of the infrared spectrum. Therefore, the $Hg_xCd_{1-x}Te$ alloy systems are of great interest as far as applications in the infrared detectors are concerned. Also, the study of the $Hg_xCd_{1-x}Te$ mixed compounds is an important source of information regarding the electronic structure of semiconductors, and it provides a better understanding of the inverted and direct band structures (a conversion from the inverted HgTe type to the direct CdTe type band structure at room temperature appears for $x=0.1$, see Ref. 1). Furthermore, if the dependence of the optical constants on the alloy composition is known, spectroscopic ellipsometry can be used to monitor the alloy composition and the thickness during growth.

There have been numerous experimental studies of the optical properties of $Hg_xCd_{1-x}Te$.[2–16] These experimental studies have mostly been limited to the reflectance or absorption spectroscopy in the narrow spectral range. The spectral ellipsometry data from Viña *et al.*[2] and Arwin and Aspnes[7] provided the experimental values for the dielectric function over a wide spectral range (1.5–6.0 eV) and for compositions $0\leqslant x\leqslant 1$. However, the experimental dielectric function data are not expressed as the analytical functions of the critical point energies or photon energy. This deficiency can be overcome by modeling. Although $Hg_xCd_{1-x}Te$ has been very interesting, studies on the modeling of its optical properties have been scarce. Works on the modeling of the optical constants of $Hg_xCd_{1-x}Te$ alloys, except for CdTe, have mostly been limited to the empirical models of the absorption edge[13,15,17–20] or quantum-mechanical calculations of the absorption coefficient at the fundamental absorption edge.[10,21] However, these approaches are valid only over a very narrow spectral range. Furthermore, the Urbach rule and its modifications give only the values of the absorption coefficient, i.e., they provide information only on the imaginary part but not the real part of the index of refraction. There was also a study of the critical points temperature dependence in $Hg_xCd_{1-x}Te$, but it did not model the dielectric function dependence on photon energy and composition.[16] Modeling for the optical constants in the wide spectral range has been performed only for CdTe.[22,23]

The main aim of modeling the optical properties of a ternary alloy is to make the calculation of the optical constants for compositions with no available experimental data possible. For that reason, the optical constants of $Al_xGa_{1-x}As$ have been extensively studied,[24–26] but such studies for $Hg_xCd_{1-x}Te$ have been lacking. Therefore, in this work, we present a model for the dielectric function of $Hg_xCd_{1-x}Te$ as a function of energy $E=\hbar\omega$, for $1.5\leqslant E\leqslant 6.0$ eV, and composition for $0\leqslant x\leqslant 1$. Also, we present a method which can accurately and reliably determine the model parameters as a function of composition $x$. The employed model represents a modification of Adachi's model for the dielectric function (MDF).[27,28] MDF is a relatively simple model which describes the optical dielectric function with terms attributed to the four energy gaps ($E_0, E_0+\Delta_0, E_1, E_1+\Delta_1$) and damped harmonic oscillators describing the contributions from the higher lying transitions [$E_0', E_2(X), E_2(\Sigma)$ etc.]. However, MDF is not very accurate, and several modifications have been proposed recently.[24,29–35]

Kim *et al.*[23,25,36] have proposed an accurate but rather complicated model, that can include either the Lorentzian or Gaussian broadening effect. Different types of broadening are accomplished by varying certain parameter in the expression of the frequency dependent damping constant. However, Kim *et al.*'s[23,25,36] model is rather intricate and employs a large number of adjustable parameters. In spite of the accurate functional form of the joint density of states (which results in complicated model equations), the behavior of their

a)Electronic mail: ehli@eee.hku.hk

 

model with the Lorentzian broadening is very similar to that of MDF, while their model with the Gaussian broadening shows a significant improvement in the accuracy. This indicates that the broadening function approximation is responsible for the large discrepancies between the MDF and the experiment in the vicinity of the fundamental band gap.[35] If we suppose that an improvement in accuracy is obtained mainly through replacing the Lorentzian broadening function with the adjustable broadening, we can retain the comparative simplicity of the model equations inherent to the MDF, while obtaining a better agreement with the experimental data at the same time.

The fact that Lorentzian broadening does not accurately describe the optical spectrum has already been recognized and discussed.[35–38] Rakić and Majewski[35] have shown that MDF with the adjustable broadening function describes accurately the dispersion and absorption of GaAs and AlAs even in the vicinity of the $E_0$, where the original model of Ozaki and Adachi[29] is highly inaccurate. Therefore, we incorporate the adjustable broadening function into MDF for CdTe[22] and apply it to modeling the optical constants of $Hg_xCd_{1-x}Te$. Our model departs from the calculations of Kimura and Adachi[22] over two more important points: we include the higher exciton states and not just the ground state excitons, and we represent the contributions of the higher lying gaps with three harmonic oscillators instead of one.

Two ways of model parameter determination of the ternary compounds are compared. The first approach is to determine the model parameters for particular compositions, and then to find the optimal function describing the dependence of the model parameters on the alloy composition $x$. The second approach is to simultaneously fit in the data sets for all available compositions in order to minimize the discrepancies between the calculated data and the experimental data over the entire energy and composition range. Our results clearly show that simultaneous fitting is needed to provide accurate values for the optical functions.

In Sec. II, a description of the model employed is given. In Sec. III, the model parameters of alloy $Hg_xCd_{1-x}Te$ as a function of composition $x$ are determined and a discussion of the results obtained is given. Finally, conclusions are drawn.

## II. MODEL OF THE DIELECTRIC FUNCTION

We shall briefly describe the applied model for the dielectric function. The dielectric function is represented by the sum of terms describing transitions at the critical points (CPs) in the joint density of states.

### A. $E_0$ and $E_0+\Delta_0$ transitions

Under the parabolic band assumption, the contributions of the three-dimensional (3D) $M_0$ CPs $E_0$ and $E_0+\Delta_0$ are given by:

$$\epsilon^{\mathrm{I}}(\omega)=AE_0^{-3/2}\left[f(\chi_0)+\frac{1}{2}\left(\frac{E_0}{E_0+\Delta_0}\right)^{3/2}f(\chi_{0s})\right], \tag{1}$$

where

$$f(y)=y^{-2}[2-(1+y)^{1/2}-(1-y)^{1/2}], \tag{2}$$

$$\chi_0=\frac{\hbar\omega+i\Gamma_0}{E_0}, \tag{3}$$

$$\chi_{0s}=\frac{\hbar\omega+i\Gamma_0}{E_0+\Delta_0}, \tag{4}$$

where $A$ and $\Gamma_0$ are the strength and the damping constants of the $E_0$ and $E_0+\Delta_0$ transitions, respectively. The exciton contributions at $E_0$ critical points are given by:

$$\epsilon_{0X}(\omega)=\sum_{m=1}^{\infty}\frac{A_0^{\mathrm{ex}}}{m^3}\frac{1}{E_0-(G_0^{\mathrm{3D}}/m^2)-E-i\Gamma_0}, \tag{5}$$

where $A_0^{\mathrm{ex}}$ is the 3D exciton strength parameter, and $G_0^{\mathrm{3D}}$ is the 3D exciton binding energy.

### B. $E_1$ and $E_1+\Delta_1$ transitions

$E_1$ and $E_1+\Delta_1$ are 3D $M_1$ CPs, but since their longitudinal effective mass is much larger than their transverse counterparts, they can be treated as 2D $M_0$ CPs.[22] For the contributions of these CPs, Adachi obtained the following expression by taking the matrix element to be constant with respect to energy:

$$\epsilon^{\mathrm{II}}(\omega)=-B_1\chi_1^{-2}\ln(1-\chi_1^2)-B_{1s}\chi_{1s}^{-2}\ln(1-\chi_{1s}^2), \tag{6}$$

where

$$\chi_1=\frac{\hbar\omega+i\Gamma_1}{E_1}, \tag{7}$$

$$\chi_{1s}=\frac{\hbar\omega+i\Gamma_1}{E_1+\Delta_1}, \tag{8}$$

$B_1(B_{1s})$ and $\Gamma_1$ are the strength and the damping constants of the $E_1$ and $E_1+\Delta_1$ transitions, respectively. The contribution of the Wannier type 2D excitons (discrete series of exciton lines at the $E_1$ and $E_1+\Delta_1$ CPs) is given by:

$$\epsilon^{\mathrm{III}}(\omega)=\sum_{n=1}^{+\infty}\frac{1}{(2n-1)^3}\left(\frac{B_{1x}}{E_1-[G_1/(2n-1)^2]-\hbar\omega-i\Gamma_1}+\frac{B_{2x}}{(E_1+\Delta_1)-[G_{1s}/(2n-1)^2]-\hbar\omega-i\Gamma_1}\right), \tag{9}$$

where $B_{1x}$ and $B_{2x}$ are the strengths and $G_1$ and $G_{1s}$ are the Rydberg energies of $E_1$ and $E_1+\Delta_1$ exciton, respectively. A summation of the excitonic terms is performed until the contribution of the next term is less than $10^{-4}$.

### C. Higher lying transitions

The origin of higher lying transitions is not completely known, since these transitions do not correspond to a single, well defined CP. There are four CPs which can contribute to the dielectric function in the investigated spectral region.[7] Kim and Sivananthan[23] considered two of these CPs, while Kimura and Adachi[22] consider only one. However, electroreflectance data indicate that three critical point structures are dominant in the 4–6 eV region,[39] and hence we employ three

damped harmonic oscillators, characterized by energy $E_j$, oscillator strength $f_j=\sqrt{C_jE_j^2}$ and damping constant $\Gamma_j$, $j=2,3,4$:

$$\epsilon^{\mathrm{IV}}(\omega)=\sum_{j=1}^{3}\frac{f_j^2}{E_j^2-(\hbar\omega)^2-i\hbar\omega\Gamma_j}. \tag{10}$$

### D. The frequency dependent damping

Let us discuss the lifetime broadening effect. The dielectric function of a solid , with its broadening described by a damping function $\gamma(s)$, is given as follows:[23]

$$\epsilon(\omega)=1+i\frac{2\hbar^2e^2}{\epsilon_0m^2}\sum_{c,v}\int J_{cv}(E)dE\left(\frac{P_{cv}(E)}{E}\right)^2 \times\left(\int_0^\infty ds\,\exp\{i[\hbar\omega-E+i\gamma(s)]s\} -\int_0^\infty ds\,\exp\{i[\hbar\omega+E+i\gamma(s)]s\}\right), \tag{11}$$

where subscripts $c$ and $v$ indicate the conduction and valence bands, respectively, $J_{cv}(E)$ is the joint density of states, and $P_{cv}(E)$ is the weighted-average matrix element of the momentum operator. If a damping function $\gamma(s)$ is expanded into a power series in $s=t/\hbar$, where $t$ is time, $\gamma(s)=\Gamma+\sigma^2s+\ldots$, one usually retains only the first term (Lorentzian broadening) or the second term (Gaussian broadening). In the former case, the broadening function $\Phi$ is given by:[35]

$$\Phi_L=-i\int_0^\infty ds\,\exp[i(\hbar\omega\pm E+i\Gamma)s]=\frac{1}{\hbar\omega\pm E+i\Gamma}. \tag{12}$$

In the latter case, the broadening function takes the following form:[35]

$$\Phi_G=-i\int_0^\infty ds\,\exp[i(\hbar\omega\pm E+i\sigma^2s)s] =-i\frac{\sqrt{\pi}}{2\sigma}\exp[-(\hbar\omega\pm E)^2/4\sigma^2] \times\left[1+\mathrm{erf}\left(i\frac{\hbar\omega\pm E}{2\sigma}\right)\right]. \tag{13}$$

Gaussian broadening represents a much better approximation for the broadening caused by electron–phonon and electron–impurities scattering.[23,35] In this case, though, the integration in equation Eq. (11) cannot be performed over the energy domain in an analytically closed form. This problem can be overcome by replacing the damping constant $\Gamma_j$ with the frequency dependent expression $\Gamma_j'(\omega)$:[23,25,36]

$$\Gamma_j'(\omega)=\Gamma_j\exp\left[-\alpha_j\left(\frac{\hbar\omega-E_j}{\Gamma_j}\right)^2\right], \tag{14}$$

where $E_j$ is the energy of a critical point at which transition occurs, and $\alpha_j$ and $\Gamma_j$ are adjustable model parameters. In this way, the shape of the line varies with the ratio of parameters $\alpha_j$ and $\Gamma_j$. This is illustrated in Fig. 1, which shows the real and imaginary parts of the optical dielectric function

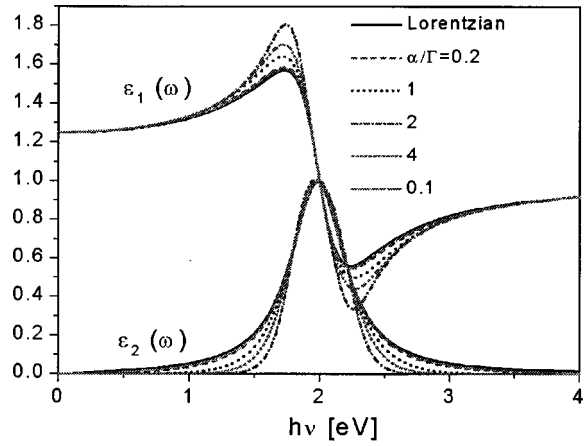


FIG. 1. Illustration of the influence of frequency dependent damping on optical constants.

versus energy for several different ratios $\alpha_j/\Gamma_j$. Line shapes range from purely Lorentzian (for $\alpha=0$) to nearly Gaussian ($\alpha=0.3$), while for large $\alpha_j/\Gamma_j$ ratios, the wings of the peak in the imaginary part of the dielectric function $\epsilon_2(\omega)$ are even narrower, thus enabling the elimination of the extended absorption tails in $\epsilon_2$ characteristics of the Lorentzian line shape. In all cases, the integration in the Eq. (11) can be performed analytically. Furthermore, in an experimentally established absorption line, the broadening mechanism, is often not clear beforehand. Therefore, one should take into account a convolution of the possible contributions of different broadening mechanisms to the shape of the absorption line.[38] Such an approach, though, would lead to a considerably involved numerical procedure. On the other hand, the frequency dependent damping concept represents a simple yet effective method to model the experimental dielectric function accurately regardless of the broadening mechanism. As there are fewer adjustable model parameters in the employed model compared with Kim *et al.*'s[23,25,36] there is no need to fix the $\alpha_j$ values. In the study of Kim *et al.*[23,25,36] parameters $\alpha_j$ were fixed to the value providing Gaussian broadening. Since no broadening mechanism is set *a priori* (both $\alpha_j$ and $\Gamma_j$ are adjustable model parameters), the model employed in this work is very flexible.

### E. Complete model for the dielectric function

The dielectric function is obtained by summing up the contributions of all the critical points described above, with $\Gamma_i$ being replaced by $\Gamma_i'(\omega)$, $i=0,1,2,3,4$:

$$\epsilon(\omega)=\epsilon_\infty+\epsilon^{\mathrm{I}}(\omega)+\epsilon_{0X}(\omega)+\epsilon^{\mathrm{II}}(\omega)+\epsilon^{\mathrm{III}}(\omega)+\epsilon^{\mathrm{IV}}(\omega), \tag{15}$$

where $\epsilon_\infty$ is the dielectric constant arising from the contributions of higher lying transitions.

## III. RESULTS AND DISCUSSION

The position of the $E_0$, $E_1$ and $E_1+\Delta_1$ CPs and their variation with composition $x$ is well established. The depen-

dence of the fundamental band gap on the composition $x$ and temperature $T$ is given by the empirical formula proposed by Hansen *et al.*:[40]

$$E_0(x,T) = -0.302 + 1.93x + 5.35(1-2x)(10^{-4})T - 0.81x^2 + 0.832x^3. \quad (16)$$

Variations of $E_1$ and $E_1+\Delta_1$ with the composition $x$ are given by the empirical relations suggested by Viña *et al.*:[2]

$$E_1(x) = 2.147 + 0.44x + 0.7x^2, \quad (17)$$

$$E_1+\Delta_1(x) = 2.778 + 0.47x + 0.6x^2. \quad (18)$$

The energies of these CPs do not represent the adjustable parameters of the model. For other model parameters, each parameter is assumed to be a cubic polynomial of composition $x$ in the form of $a_{0i}(1-x)+(a_{1i}+a_{2i}x)x(1-x)+a_{3i}x$. No attempt was made to constrain the values during the fitting procedure, except for the added penalty function when the resulting parameter value was negative. The following objective function was employed:

$$F = \sum_{j=1}^{j=N_x} \sum_{i=1}^{i=N_p} \left( \left| \frac{\epsilon_1(\omega_i,x_j) - \epsilon_1^{\text{expt}}(\omega_i,x_j)}{\epsilon_1^{\text{expt}}(\omega_i,x_j)} \right| + \left| \frac{\epsilon_2(\omega_i,x_j) - \epsilon_2^{\text{expt}}(\omega_i,x_j)}{\epsilon_2^{\text{expt}}(\omega_i,x_j)} \right| \right)^2, \quad (19)$$

where $N_p$ is the number of experimental points, $N_x$ is the number of different compositions and $\epsilon_1(\omega_i,x_j)$, $\epsilon_2(\omega_i,x_j)$ are the calculated values of the real and imaginary parts of the dielectric constant at frequency $\omega_i$ for composition $x_j$, while $\epsilon_1^{\text{expt}}(\omega_i,x_j)$, $\epsilon_2^{\text{expt}}(\omega_i,x_j)$ are the corresponding experimental values. The experimental data employed for the model parameter determination are tabulated in Ref. 41, and they consist of the room temperature spectral ellipsometry data measured by Viña *et al.*[2] and Arwin and Aspnes.[7] The objective function was minimized by acceptance probability controlled simulated annealing algorithm with the adaptive move-generation procedure.[42,43]

The details of the fitting procedures are as follows. In this work, we compare two approaches: the determination of the optimal cubic polynomial describing the composition dependence of model parameters obtained by fitting in the data for each composition separately and by fitting in all available compositions simultaneously. In the first case, the experimental data for individual compositions were fitted in separately, and the model parameters obtained are given in Table I. A comparison with the calculations of Kimura and Adachi[22] for CdTe is shown in Fig. 2. It can be observed that our model (solid line) is superior to that of Kimura and Adachi[22] (broken line) in terms of the agreement with the experimental data (circles) obtained. Then, the optimal cubic polynomial describing the composition dependence of each parameter was determined. However, it was found that such a method can significantly degrade the accuracy of the estimated dielectric function. This has already been pointed out by Terry,[26] who then used the simultaneous fitting method to determine the parameters of the damped harmonic oscillator model for $Al_xGa_{1-x}As$. Still, most other authors prefer the approach of finding the optimal cubic polynomial after estimating the parameters for each composition separately, as this is less time-consuming and demands fewer computer resources.

TABLE I. Model parameter values obtained by individual fitting.

| Composition | 0.0 | 0.2 | 0.29 | 0.43 | 0.76 | 0.86 | 0.91 | 1.0 |
|---|---|---|---|---|---|---|---|---|
| $\epsilon_\infty$ | 1.665 | 1.512 | 1.710 | 1.938 | 1.260 | 1.544 | 1.404 | 1.252 |
| $A$ ($eV^{1.5}$) | 3.100 | 0.188 | 0.799 | 1.003 | 2.753 | 4.818 | 5.696 | 5.098 |
| $10\times\Gamma_0$ (eV) | 0.025 | 0.435 | 0.039 | 0.358 | 0.134 | 0.033 | 0.471 | 0.487 |
| $\alpha_0$ | 3.561 | 6.184 | 3.286 | 0.585 | 7.314 | 7.100 | 6.090 | 1.531 |
| $B_1$ (eV) | 1.320 | 1.414 | 1.882 | 1.726 | 1.285 | 1.689 | 1.672 | 1.816 |
| $B_{1s}$ (eV) | 0.240 | 0.407 | 0.300 | 0.156 | 1.788 | 1.561 | 1.713 | 1.055 |
| $B_{1x}$ (eV) | 0.453 | 0.751 | 0.785 | 0.746 | 0.697 | 1.415 | 1.345 | 1.029 |
| $B_{2x}$ (eV) | 0.248 | 0.401 | 0.448 | 0.356 | 0.549 | 0.807 | 0.821 | 0.666 |
| $10\times\Gamma_1$ (eV) | 1.349 | 2.017 | 2.276 | 2.307 | 2.465 | 3.027 | 3.055 | 1.904 |
| $\alpha_1$ | 0.090 | 0.012 | 0.040 | 0.123 | 0.030 | 0.046 | 0.024 | 0.013 |
| $f_2$ (eV) | 4.526 | 6.252 | 5.648 | 4.407 | 4.618 | 3.660 | 3.894 | 5.232 |
| $\Gamma_2$ (eV) | 1.167 | 1.412 | 1.296 | 1.082 | 0.945 | 0.722 | 0.715 | 0.734 |
| $\alpha_2$ | 0.397 | 0.058 | 0.039 | 0.029 | 0.014 | 0.002 | 0.377 | 0.022 |
| $E_2$ (eV) | 4.559 | 4.717 | 4.778 | 4.798 | 4.959 | 5.028 | 5.004 | 5.089 |
| $f_3$ (eV) | 6.147 | 6.114 | 3.238 | 4.422 | 3.401 | 1.982 | 0.439 | 1.861 |
| $\Gamma_3$ (eV) | 1.946 | 1.804 | 0.696 | 3.726 | 2.266 | 0.925 | 0.139 | 0.087 |
| $\alpha_3$ | 0.173 | 0.070 | 0.001 | 0.081 | 0.079 | 0.096 | 0.018 | 0.160 |
| $E_3$ (eV) | 6.499 | 6.772 | 6.427 | 5.432 | 2.286 | 4.714 | 14.00 | 6.356 |
| $f_4$ (eV) | 8.750 | 6.555 | 8.424 | 8.122 | 3.673 | 1.644 | 1.728 | 2.033 |
| $\Gamma_4$ (eV) | 4.146 | 3.027 | 5.491 | 4.854 | 1.365 | 0.830 | 1.056 | 0.929 |
| $\alpha_4$ | 0.797 | 0.069 | 0.399 | 0.066 | 0.001 | 3.102 | 3.999 | 0.014 |
| $E_4$ (eV) | 2.919 | 3.053 | 3.882 | 3.905 | 2.816 | 2.584 | 2.807 | 2.890 |
| $A_0^{\text{ex}}$ (eV) | 0.003 | 0.020 | 0.001 | 0.011 | 0.002 | 0.001 | 0.001 | 0.010 |
| $G_0^{\text{3D}}$ (eV) | 0.002 | 0.005 | 0.003 | 0.013 | 0.030 | 0.018 | 0.022 | 0.001 |
| $G_1$ (eV) | 0.054 | 0.005 | 0.001 | 0.0001 | 0.027 | 0.076 | 0.010 | 0.001 |
| $G_{1s}$ (eV) | 0.057 | 0.026 | 0.001 | 0.001 | 0.120 | 0.143 | 0.069 | 0.013 |
| $E_0+\Delta_0$ (eV) | 0.654 | 0.946 | 1.567 | 1.544 | 1.910 | 1.945 | 2.119 | 2.456 |

Simultaneous fitting for all the available compositions was employed next. This procedure was obviously more demanding on the optimization algorithm and also more computationally intensive. The number of data points has been increased by an order of magnitude, while the number of

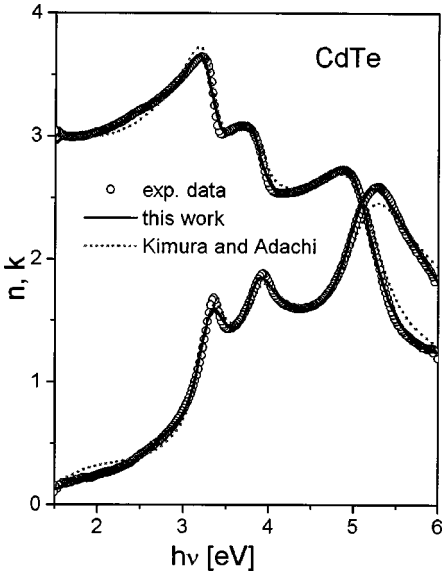


FIG. 2. The real and imaginary parts of the index of refraction of CdTe: (circles) experimental data, (solid line) this work, (dotted line) Ref. 22.

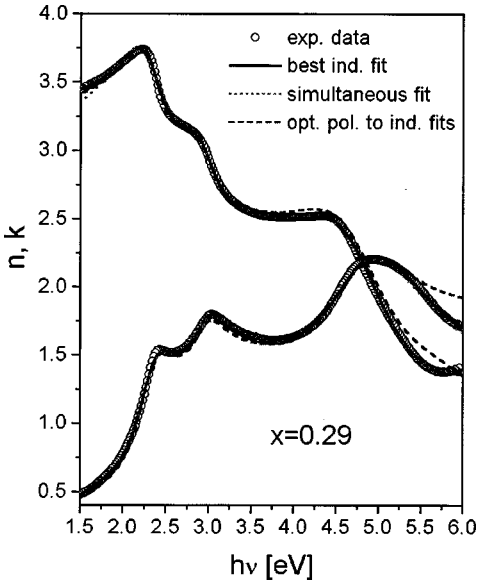


FIG. 3. The real and imaginary parts of the index of refraction for $x=0.29$ as a function of energy; (circles) experimental data, (solid line) results obtained by simultaneous fit to all compositions, (dotted line) best individual fit for $x=0.29$, (dashed line) results corresponding to model parameters calculated by optimal cubic polynomial approximating points obtained by fitting each composition separately.

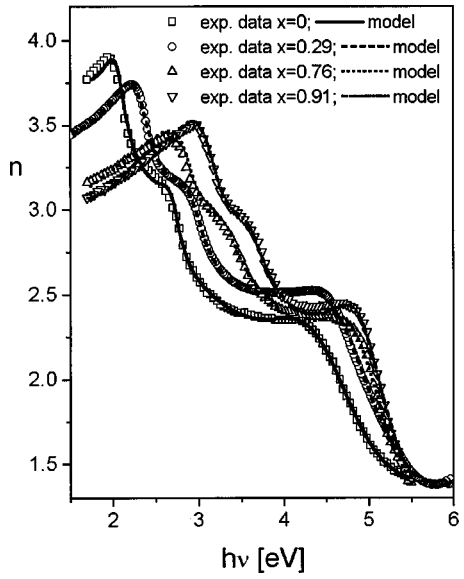


FIG. 4. The real part of the index of refraction as a function of energy for compositions $x=0.0$, 0.29, 0.76, and 0.91.

fitting parameters has been increased four times at the same time. Nevertheless, this computational effort is justified by the improved accuracy of the cubic polynomial describing parameter dependence on composition $x$. This is illustrated in Fig. 3, which depicts three different calculated curves: the solid line is the result for the best simultaneous fit across all material compositions; the dotted line shows the best fit for that particular composition. The broken line is obtained using the cubic polynomial (cubic polynomial fit to parameters determined in individual fits) instead of the parameters obtained for a particular $x$. A deterioration of the fit quality will result if the optimal cubic polynomial is found after the parameters for each composition are estimated separately. For that reason, the simulatenous approach to model the parameter estimation for the ternary alloy should be favored.

The model parameter estimation is performed as follows. Model parameters $a_{0i}$ and $a_{1i}$ corresponding to compositions $x=0.0$ and $x=1.0$, respectively, are first obtained by mini-

TABLE II. Parameter values obtained by simultaneous fitting method.

| Parameter | $a_{0i}$ | $a_{1i}$ | $a_{2i}$ | $a_{3i}$ |
|---|---|---|---|---|
| $\epsilon_\infty$ | 1.665 | 0.644 | −1.339 | 1.252 |
| $A$ eV$^{1.5}$ | 3.100 | −6.988 | 1.974 | 5.098 |
| $10\times\Gamma_0$ (eV) | 0.025 | 6.119 | −1.784 | 0.487 |
| $\alpha_0$ | 3.561 | −4.310 | 3.143 | 1.531 |
| $B_1$ (eV) | 1.320 | 5.542 | −3.599 | 1.816 |
| $B_{1s}$ (eV) | 0.240 | 4.289 | −4.040 | 1.055 |
| $B_{1x}$ (eV) | 0.453 | 2.604 | −0.066 | 1.029 |
| $B_{2x}$ (eV) | 0.248 | 1.100 | 0.373 | 0.666 |
| $10\times\Gamma_1$ (eV) | 1.349 | 3.421 | 10.095 | 1.904 |
| $\alpha_1$ | 0.090 | −0.461 | 0.614 | 0.013 |
| $f_2$ (eV) | 4.526 | 6.421 | −9.926 | 5.232 |
| $\Gamma_2$ (eV) | 1.167 | 0.873 | 0.481 | 0.734 |
| $\alpha_2$ | 0.397 | −0.010 | 0.119 | 0.022 |
| $E_2$ (eV) | 4.559 | 0.506 | −0.856 | 5.089 |
| $f_3$ (eV) | 6.147 | 6.139 | −8.472 | 1.861 |
| $\Gamma_3$ (eV) | 1.946 | 0.808 | −0.944 | 0.087 |
| $\alpha_3$ | 0.173 | −1.905 | 4.202 | 0.160 |
| $E_3$ (eV) | 6.499 | 1.564 | 1.374 | 6.356 |
| $f_4$ (eV) | 8.750 | ⋯ | ⋯ | 2.033 |
| $\Gamma_4$ (eV) | 4.146 | −14.678 | 7.230 | 0.929 |
| $\alpha_4$ | 0.797 | 8.128 | −13.712 | 0.014 |
| $E_4$ (eV) | 2.919 | 3.472 | −6.331 | 2.890 |
| $A_0^{ex}$ (eV) | 0.003 | 2.505 | −3.000 | 0.010 |
| $G_0^{3D}$ (eV) | 0.002 | 3.084 | −3.589 | 0.001 |
| $G_1$ (eV) | 0.054 | −0.378 | 0.664 | 0.001 |
| $G_{1s}$ (eV) | 0.057 | −0.212 | 0.384 | 0.013 |
| $E_0+\Delta_0$ (eV) | 0.654 | 0.778 | −2.626 | 2.456 |

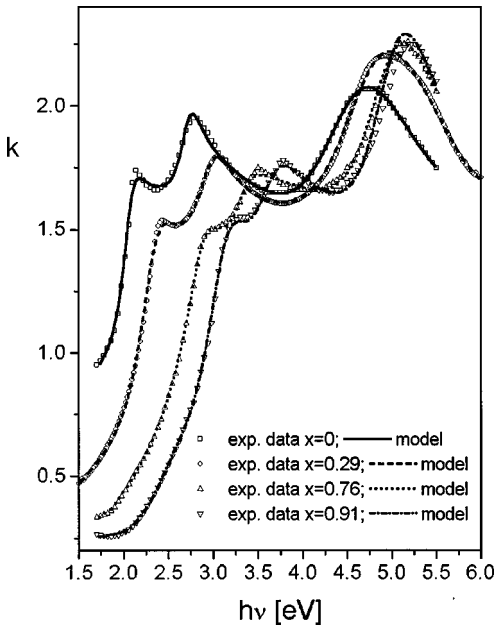


FIG. 5. The imaginary part of the index of refraction as a function of energy for compositions $x=0.0$, 0.29, 0.76 and 0.91.

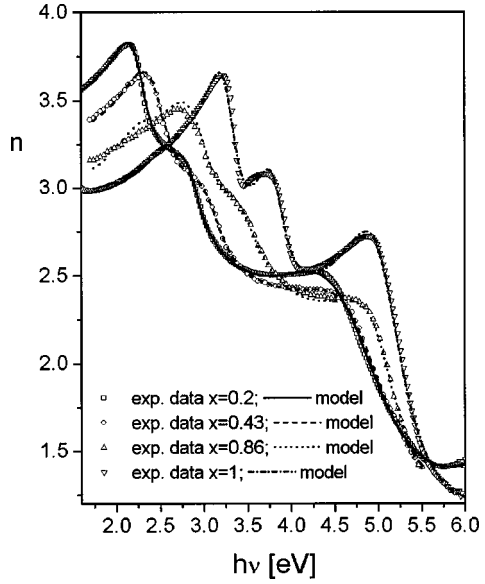


FIG. 6. The real part of the index of refraction as a function of energy for compositions $x=0.2$, 0.43, 0.86 and 1.0.

mizing the discrepancy between the calculated and experimental data for those compositions. The main reason for estimating these parameters separately is that the optical properties of the binary materials (HgTe and CdTe) have been more extensively studied, hence the data can be considered to be more reliable. After determinated $a_{0i}$ and $a_{1i}$, parameters $a_{2i}$ and $a_{3i}$ are obtained by minimizing the discrepancies between the calculated data and the experimental data for all available compositions $0<x<1$. The resulting coefficients are given in Table II.

Figures 4 and 5 show the real and imaginary parts of the index of refraction versus energy, respectively, for compositions 0.0, 0.29, 0.76 and 0.91. Figures 6 and 7 depict the

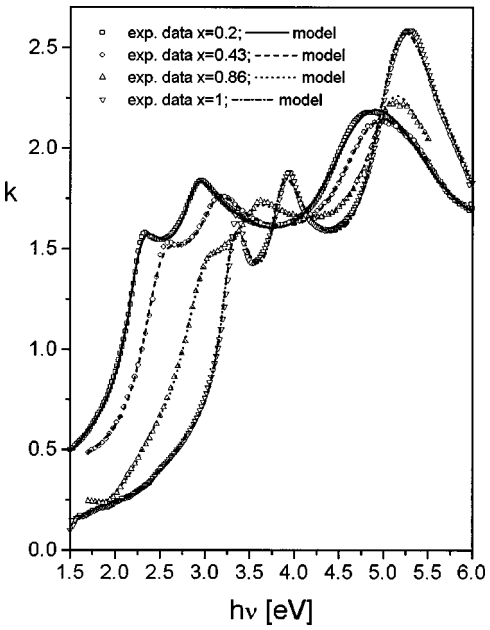


FIG. 7. The imaginary part of the index of refraction as a function of energy for compositions $x=0.2$, 0.43, 0.86 and 1.0.

TABLE III. Obtained rms errors for $n$ and $k$.

| Method | 1 | 2 | 3 |
|---|---|---|---|
| 0.0 | 0.6% 0.7% | 4.5% 2.2% | 0.6% 0.7% |
| 0.2 | 0.5% 0.6% | 2.1% 2.6% | 0.9% 1.5% |
| 0.29 | 0.5% 0.7% | 3.0% 3.8% | 0.8% 1.5% |
| 0.43 | 0.4% 0.8% | 2.7% 5.5% | 1.4% 2.6% |
| 0.76 | 0.9% 0.9% | 4.7% 5.5% | 1.7% 2.2% |
| 0.86 | 0.9% 1.4% | 2.2% 4.2% | 1.5% 3.0% |
| 0.91 | 1.2% 1.5% | 2.1% 6.9% | 2.4% 5.8% |
| 1.0 | 1.0% 2.8% | 2.3% 8.4% | 1.0% 2.8% |

respective energy dependence of $n$ and $k$ for compositions $x=0.2$, 0.43, 0.86 and 1.0. The relative rms errors obtained for the real and imaginary parts of the index of refraction for different fitting methods (1—best individual fit; 2—cubic polynomial fit to parameters obtained in individual fits; 3—simultaneous fit) are given in Table III. An excellent agreement with the experimental data is obtained for the entire investigated spectral region and for all compositions. Results obtained by the simultaneous fitting method are similar to those obtained by the best individual fit, except for $x=0.91$, where the simultaneous fit produces a slightly higher discrepancy from the experimental data.

## IV. CONCLUSION

The optical properties of $Hg_xCd_{1-x}Te$ are modeled in the 1.5–6 eV range for all compositions $0\leqslant x\leqslant 1$. An extension of the Adachi's model employing the adjustable broadening function rather than the conventional Lorentzian one is used. Two different approaches for modeling the optical constants of ternary alloys are compared and discussed. Using the simultaneous fitting method and a global optimization routine, an excellent agreement with the experimental data is obtained for all compositions.

## ACKNOWLEDGMENTS

This work was supported by the Research Grant Council (RGC) Earmarked Grant of Hong Kong. A.B.D. acknowledges the support of a William Mong Postdoctoral Fellowship of the Faculty of Engineering for this work.

[1] J. Stankiewicz and W. Giriat, Phys. Status Solidi B **49**, 387 (1972).
[2] L. Viña, C. Umbach, M. Cardona, and L. Vodopyanov, Phys. Rev. B **29**, 6752 (1984).
[3] M. Cardona, J. Appl. Phys. **32**, 2151 (1961).
[4] M. D. Blue, Phys. Rev. **134**, A226 (1964).
[5] M. Grynberg, R. L. Toullec, and M. Balkanski, Phys. Rev. B **9**, 517 (1974).
[6] A. Rodzik and A. Kisiel, J. Phys. C **16**, 203 (1983).
[7] H. Arwin and D. E. Aspnes, J. Vac. Sci. Technol. A **2**, 1316 (1984).
[8] W. D. Lawson, S. Nielsen, E. H. Putley, and A. S. Yung, J. Phys. Chem. Solids **9**, 325 (1959).
[9] T. N. Casselman and G. L. Hansen, J. Vac. Sci. Technol. A **1**, 1682 (1983).
[10] W. W. Anderson, Infrared Phys. **20**, 363 (1980).
[11] D. T. F. Marple and H. Ehrenreich, Phys. Rev. Lett. **8**, 87 (1962).
[12] K. Liu, J. H. Chu, and D. Y. Tang, J. Appl. Phys. **75**, 4176 (1994).
[13] J. H. Chu, Z. Y. Mi, and D. Y. Tang, J. Appl. Phys. **71**, 3955 (1992).
[14] D. T. F. Marple, Phys. Rev. **150**, 728 (1966).
[15] J. H. Chu, B. Li, K. Liu, and D. Y. Tang, J. Appl. Phys. **75**, 1234 (1994).
[16] C. C. Kim and S. Sivananthan, J. Electron. Mater. **26**, 561 (1997).

[17] E. Finkman and S. E. Schacham, J. Appl. Phys. **56**, 2896 (1984).
[18] J. H. Chu, S. C. Hu, and D. Y. Tang, Appl. Phys. Lett. **43**, 1064 (1983).
[19] E. Finkman and Y. Nemirovsky, J. Appl. Phys. **50**, 4356 (1979).
[20] V. Nathan, J. Appl. Phys. **83**, 2812 (1998).
[21] J. L. Schmit, J. Appl. Phys. **41**, 2876 (1970).
[22] T. Kimura and S. Adachi, Jpn. J. Appl. Phys., Part 1 **32**, 2740 (1993).
[23] C. C. Kim and S. Sivananthan, J. Appl. Phys. **78**, 4003 (1995).
[24] S. Adachi, Phys. Rev. B **38**, 12345 (1989).
[25] C. C. Kim, J. W. Garland, H. Abad, and P. M. Raccah, Phys. Rev. B **47**, 1876 (1993).
[26] F. L. Terry, Jr., J. Appl. Phys. **70**, 409 (1991).
[27] S. Adachi, J. Appl. Phys. **53**, 5863 (1982).
[28] S. Adachi, J. Appl. Phys. **58**, R1 (1985).
[29] S. Ozaki and S. Adachi, J. Appl. Phys. **78**, 3380 (1995).
[30] D. W. Jenkins, J. Appl. Phys. **68**, 1848 (1990).
[31] S. Adachi, T. Kimura, and N. Suzuki, J. Appl. Phys. **74**, 3435 (1993).
[32] R. J. Deri and M. A. Emanuel, J. Appl. Phys. **74**, 3435 (1993).
[33] Y. Kokubo and I. Ohto, J. Appl. Phys. **81**, 2042 (1997).
[34] J. Zheng, C.-H. Lin, and C. H. Kuo, J. Appl. Phys. **82**, 792 (1997).
[35] A. D. Rakić and M. L. Majewski, J. Appl. Phys. **80**, 5509 (1996).
[36] C. C. Kim, J. W. Garland, H. Abad, and P. M. Raccah, Phys. Rev. B **45**, 11749 (1992).
[37] O. Stenzel, R. Petrich, W. Scharff, A. Tikhonravov, and V. Hopfe, Thin Solid Films **207**, 324 (1992).
[38] A. Franke, A. Stendal, O. Stenzel, and C. von Borczyskowski, Pure Appl. Opt. **5**, 845 (1996).
[39] A. Moritani, K. Taniguchi, C. Hamaguchi, and J. Nakai, J. Phys. Soc. Jpn. **34**, 79 (1973).
[40] G. L. Hansen, J. L. Schmit, and T. N. Casselman, J. Appl. Phys. **53**, 7099 (1982).
[41] P. M. Armitharaj, in *Handbook of Optical Constants of Solids II*, edited by E. D. Palik (Academic, San Diego, 1991), pp. 655–689.
[42] A. D. Rakić, J. M. Elazar, and A. B. Djurišić, Phys. Rev. E **52**, 6862 (1995).
[43] A. B. Djurišić, A. D. Rakić, and J. M. Elazar, Phys. Rev. E **55**, 4797 (1997).